

CHEERS: A tool for Correlated Hole-Electron Evolution from Real-time Simulations

E. Perfetto^{1,2} and G. Stefanucci^{2,3}

¹*CNR-ISM, Division of Ultrafast Processes in Materials (FLASHit),*

Area della ricerca di Roma 1, Monterotondo Scalo, Italy

²*Dipartimento di Fisica, Università di Roma Tor Vergata,*

Via della Ricerca Scientifica, 00133 Rome, Italy

³*INFN, Sezione di Roma Tor Vergata, Via della Ricerca Scientifica 1, 00133 Roma, Italy*

(Dated: March 13, 2022)

We put forward a practical nonequilibrium Green's function (NEGF) scheme to perform real-time evolutions of many-body interacting systems driven out of equilibrium by external fields. CHEERS is a computational tool to solve the NEGF equation of motion in the so called generalized Kadanoff-Baym ansatz and it can be used for model systems as well as first-principles Hamiltonians. Dynamical correlation (or memory) effects are added to the Hartree-Fock dynamics through a many-body self-energy. Applications to time-dependent quantum transport, time-resolved photoabsorption and other ultrafast phenomena are discussed.

I. INTRODUCTION

Although the laws of quantum mechanics have been formulated almost a century ago, the behavior of quantum matter under (extreme) nonequilibrium conditions remains still largely unexplored. Modern advances in laser technology [1–3] make today possible to film, with an unprecedented time resolution, the genesis and development of photoemission processes, exciton formation, charge transfers, charge migrations, Auger decays and other ultrafast phenomena. This is the realm of attosecond physics which calls for accurate theories and efficient numerical schemes to predict the evolution of many-body quantum systems.

One of the most versatile formalism to deal with the quantum many-body problem is the diagrammatic Green's function theory. The extension to out-of-equilibrium situations is known as the Non-Equilibrium Green's Function (NEGF) theory [4–6] and the fundamental equations, known as Kadanoff-Baym equations (KBE), date back to the mid sixties [7–9]. Despite the enormous advance in computational capabilities the KBE are still rather burdensome to solve numerically. In fact, their implementations have been so far restricted to atoms, diatomic molecules or model systems [10–19]. In the mid-1980s Lipavsky *et al.* [20] proposed the so called Generalized Kadanoff-Baym Ansatz (GKBA) to collapse the KBE for the two-times Green's function into a single equation for the one-time one-particle density matrix, thus drastically reducing the computational cost. The GKBA is exact in the Hartree-Fock (HF) approximation and it is expected to be accurate when the average time between two consecutive collisions is longer than the quasiparticle decay time (see Ref. [21] for a recent discussion).

The appealing feature of the GKBA is that the NEGF formalism is converted into a time-dependent density-matrix functional theory [22–28] which shares a fundamental property with many-body perturbation theory, i.e., the systematic inclusion of correlations through a

proper selection of self-energy diagrams. Recent applications of the NEGF+GKBA approach include the nonequilibrium dynamics [29, 30] and many-body localization [31] of Hubbard clusters, equilibrium absorption of sodium clusters [32], transient absorption [33–35] and carrier dynamics [36, 37] of semiconductors.

In this work we describe CHEERS, a first-principles numerical tool based on NEGF+GKBA to simulate the time evolution of interacting systems. CHEERS time-evolutions contain dynamical correlation (or memory) effects responsible for double (and multiple) excitations, decoherence-induced charge separation, Auger decays, shake-up dynamics, image-charge renormalizations, etc. Standard time-dependent HF simulations are recovered by simply switching off the effects of correlations. CHEERS has been already used to study the charge dynamics of model molecular junctions [21], the transient photoabsorption spectrum of noble gas atoms [38], the formation of charge-transfer excitons and their subsequent separation in donor-acceptor complexes [39], the attosecond pulse-induced charge migration in the phenylalanine aminoacid [40] and time-resolved Auger decays [41].

The paper is organized as follows. In Section II we discuss the physical systems of interest and write down the many-body Hamiltonian to describe them. The theoretical framework based on NEGF and GKBA is outlined in Section III along with the NEGF equation of motion solved by CHEERS. In Section IV we list the observable quantities accessible from the solution of the NEGF equation. A description of the implementation details is given in Section V. Conclusions and outlooks are drawn in Section VI.

II. PHYSICAL SYSTEMS

We consider a quantum system with a finite number of nuclei. For the time being we fix the nuclear coordinates and focus on the electronic degrees of freedom. Let $\{\varphi_i(\mathbf{x})\}$ be a set of localized orthonormal spin-orbitals

sued to describe the equilibrium and nonequilibrium properties of the bound electrons. In our notation $\mathbf{x} = \mathbf{r}\sigma$ comprises a spatial coordinate \mathbf{r} and a spin-projection σ , and $\varphi_i(\mathbf{x}) = \langle i|\mathbf{x}\rangle$. The localized states could be generated by orthonormalizing a set of Slater-type orbitals (STO) or Gaussian-type orbitals (GTO) centered around each nucleus or they could be the bound Hartree-Fock (HF) orbitals or the bound Kohn-Sham (KS) orbitals resulting from some self-consistent HF or KS calculation respectively. We will give more details on the possible choice of the basis set in Section V. For each spin-orbital φ_i we define the corresponding annihilation and creation operator \hat{c}_i and \hat{c}_i^\dagger . The equilibrium Hamiltonian of the system in second quantization then reads

$$\hat{H}_{\text{sys}}^{\text{eq}} = \sum_{ij} h_{ij}^{\text{eq}} \hat{c}_i^\dagger \hat{c}_j + \frac{1}{2} \sum_{ijmn} v_{ijmn} \hat{c}_i^\dagger \hat{c}_j^\dagger \hat{c}_m \hat{c}_n. \quad (1)$$

Here h_{ij}^{eq} are the matrix elements of the single-particle Hamiltonian (atomic units are used throughout):

$$h_{ij}^{\text{eq}} \equiv \langle i | \frac{\hat{p}^2}{2} + \hat{V}_n + \hat{V}_{\text{SO}} | j \rangle, \quad (2)$$

with \hat{V}_n the nuclear potential and \hat{V}_{SO} the spin-orbit interaction potential. The second term in Eq. (1) describes the electron-electron interaction with Coulomb integrals

$$v_{ijmn} \equiv \int d\mathbf{x} d\mathbf{x}' \frac{\varphi_i^*(\mathbf{x}) \varphi_j^*(\mathbf{x}') \varphi_m(\mathbf{x}') \varphi_n(\mathbf{x})}{|\mathbf{r} - \mathbf{r}'|}, \quad (3)$$

where $\int d\mathbf{x} = \int d\mathbf{r} \sum_\sigma$.

We are interested in studying the quantum evolution induced by an external electromagnetic field with spatial variations on length-scales much longer than the linear dimension of the system. For nanometer-sized molecules this condition implies photon energies up to 1 keV and hence the possibility of photoionization. To describe photoionization processes it is necessary to extend the localized basis and include delocalized spin-orbitals $\{\varphi_\mu(\mathbf{x})\}$ for electrons in the continuum. Without loss of generality, we choose the φ_μ 's as eigenstates of the free-particle Hamiltonian far away from the system boundaries and we denote by ϵ_μ their energy. We also require that the φ_μ 's are orthogonal to the φ_i 's and orthonormal between themselves, i.e., $\langle \mu | \mu' \rangle = \delta_{\mu\mu'}$. An example of how to construct the φ_μ 's is given in Section V. We discard the Coulomb interaction between two electrons in the continuum since for weak pulses double ionization is strongly suppressed. Of course, if X-rays are used then a second (Auger) electron can be ejected. As we discuss in Section III, in this case the approximation is justified provided that the photoelectron and the Auger electron have different energies. The continuum Hamiltonian then reads

$$\hat{H}_{\text{cont}} = \sum_\mu \epsilon_\mu \hat{c}_\mu^\dagger \hat{c}_\mu. \quad (4)$$

Taking into account that the electric field \mathbf{E} is uniform for all localized states, we can write the interaction Hamiltonian between light and matter as

$$\hat{H}^{\mathbf{E}}(t) = \hat{H}_{\text{sys}}^{\mathbf{E}}(t) + \hat{H}_{\text{ion}}^{\mathbf{E}}(t), \quad (5)$$

where

$$\hat{H}_{\text{sys}}^{\mathbf{E}}(t) = \mathbf{E}(t) \cdot \sum_{ij} \mathbf{d}_{ij} \hat{c}_i^\dagger \hat{c}_j \quad (6)$$

is the part responsible for reshuffling the electrons between localized states whereas

$$\hat{H}_{\text{ion}}^{\mathbf{E}}(t) = \mathbf{E}(t) \cdot \sum_{i\mu} \left(\mathbf{d}_{i\mu} \hat{c}_i^\dagger \hat{c}_\mu + \text{h.c.} \right) \quad (7)$$

is the part responsible for photoionization processes. In Eqs. (6) and (7) the vector of matrices \mathbf{d} is the dipole moment defined as

$$\mathbf{d}_{ab} = \int d\mathbf{x} \varphi_a^*(\mathbf{x}) \mathbf{r} \varphi_b(\mathbf{x}), \quad (8)$$

where a and b are indices either in the localized $\{i\}$ or delocalized $\{\mu\}$ sector. In Eq. (5) we are discarding transitions $\mu \rightarrow \mu'$ between delocalized electrons since we are mainly concerned with ultrafast fields (by the time the population of a μ -state becomes relevant the electric field vanishes).

During the first few femtoseconds after ionization from a (semi) core state, the Auger decay is one of the most relevant recombination channels. To account for the Auger effect in our description (and hence to deal with soft X-ray pulses too) we include the Coulomb matrix elements responsible for two localized (valence) electrons to scatter in one localized (core) electron and one delocalized (continuum) electron. In second quantization the Auger interaction Hamiltonian reads

$$\hat{H}_{\text{Auger}} = \sum_{ijm} \sum_\mu v_{ijm\mu}^A \left(\hat{c}_i^\dagger \hat{c}_j^\dagger \hat{c}_m \hat{c}_\mu + \text{h.c.} \right), \quad (9)$$

where the Coulomb integrals $v_{ijm\mu}^A$ are defined as in Eq. (3) with $\varphi_n \rightarrow \varphi_\mu$.

In CHEERS the quantum system can also be contacted to metallic leads with which to exchange electrons and energy. Arbitrary time-dependent voltages can be applied to the leads to study transient currents, steady-states, AC responses or other kind of transport properties. It is also possible to switch on a thermomechanical field [42] to calculate time-dependent thermal currents [43–45]. The combination of applied voltages and external laser pulses $\mathbf{E}(t)$ can instead be used to access the optical properties of current-carrying molecular junctions [46]. In all cases the leads are treated as noninteracting semi-infinite crystals with a finite cross section and described in terms of semi-infinite Bloch states $\varphi_{\alpha k}(\mathbf{x})$, where α is the lead index and k specifies the energy $\epsilon_{\alpha k}$ of the Bloch state. The Bloch states have to be orthogonal to both the φ_i 's

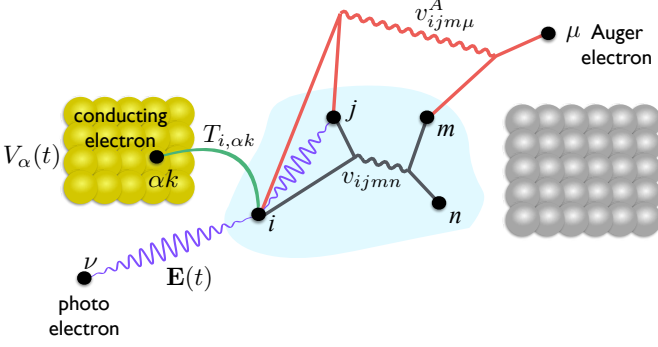


FIG. 1: Illustration of the possible physical effects that can be addressed with the Hamiltonian in Eq. (12).

and the φ_μ 's. Thus, in a quantum transport setup the μ -states are the free-particle continuum states of the quantum system contacted to leads. The second-quantized form of the leads Hamiltonian is

$$\hat{H}_{\text{lead}}(t) = \sum_{\alpha} \sum_k \Phi_{\alpha}(t) (\epsilon_{\alpha k} + V_{\alpha}(t)) \hat{c}_{\alpha k}^{\dagger} \hat{c}_{\alpha k}, \quad (10)$$

where $V_{\alpha}(t)$ is the applied voltage and $\Phi_{\alpha}(t) = T_{\alpha}(t)/T$ is the ratio between the temperature at time t and the equilibrium temperature (the thermomechanical field is therefore $\Psi_{\alpha} = \Phi_{\alpha} - 1$). The contact Hamiltonian responsible for electron tunneling has the general form

$$\hat{H}_{\text{tun}} = \sum_{i, \alpha k} \left(T_{i, \alpha k} \hat{c}_i^{\dagger} \hat{c}_{\alpha k} + \text{h.c.} \right), \quad (11)$$

where $T_{i, \alpha k}$ is the tunneling amplitude, i.e., the matrix element of the single-particle Hamiltonian, between the states φ_i and $\varphi_{\alpha k}$.

To summarize, the full Hamiltonian has the form

$$\hat{H} = \hat{H}_{\text{sys}} + \hat{H}_{\text{cont}} + \hat{H}_{\text{lead}} + \hat{H}_{\text{ion}}^{\mathbf{E}} + \hat{H}_{\text{Auger}} + \hat{H}_{\text{tun}}, \quad (12)$$

where

$$\hat{H}_{\text{sys}} = \hat{H}_{\text{sys}}^{\text{eq}} + \hat{H}_{\text{sys}}^{\mathbf{E}}. \quad (13)$$

In Fig. 1 we show an illustration of the physics that can be studied with the Hamiltonian in Eq. (12).

III. GREEN'S FUNCTION FORMULATION

Although the full Hamiltonian in Eq. (12) includes only the Auger scattering between bound electrons and continuum electrons, neglects the electron-electron interaction in the leads and discards the effects of $\mathbf{E}(t)$ on the free-particle Hamiltonian of the continuum states, the general solution of the problem is still challenging. To make some progress we restrict the physical situations of interest. In experiments the momentum of the photoelectron is often well separated from the momentum of the Auger electron. Having in mind this type of experiments

we take the set \mathcal{S}_{ion} of photoelectron states and the set $\mathcal{S}_{\text{Auger}}$ of Auger-electron states as two disjoint sets. This implies that in Eq. (7) we can restrict the sum over μ to states with $\mu \in \mathcal{S}_{\text{ion}}$ and, similarly, in Eq. (9) we can restrict the sum over μ to states with $\mu \in \mathcal{S}_{\text{Auger}}$.

A. NEGF equations

The method of choice to investigate the electron dynamics is the Non-Equilibrium Green's Function (NEGF) approach [4–6]. The Green's function $G_{ij}(z, z')$ with times z, z' on the Keldysh contour and indices i, j in the localized sector satisfies the equation of motion

$$\left[i \frac{d}{dz} - h_{\text{HF}}(z) \right] G(z, z') = \delta(z, z') + \mathcal{I}_{\text{emb}}(z, z') + \mathcal{I}_{\text{ion}}(z, z') + \mathcal{I}_{\text{coll}}(z, z') + \mathcal{I}_{\text{Auger}}(z, z') \quad (14)$$

and its adjoint. Let us discuss the quantities in Eq. (14). The matrix h_{HF} is the single-particle Hartree-Fock (HF) Hamiltonian with elements

$$h_{\text{HF}, ij}(z) \equiv h_{ij}^{\text{eq}} + V_{\text{HF}, ij}(z) + \mathbf{E}(z) \cdot \mathbf{d}_{ij}, \quad (15)$$

where the HF potential

$$V_{\text{HF}, ij}(z) \equiv \sum_{mn} \rho_{nm}(z) w_{imnj}(z) \quad (16)$$

is expressed in terms of the one-particle density matrix

$$\rho_{nm}(z) \equiv -i G_{nm}(z, z^+) \quad (17)$$

and the difference between the direct and exchange Coulomb integrals

$$w_{imnj}(z) \equiv v_{imnj}(z) - v_{imjn}(z). \quad (18)$$

Hereafter we consider the more general case of a time-dependent interaction $v = v(z)$, useful to deal with adiabatic switching, interaction quenches, etc..

The *embedding/ionization* integral

$$\mathcal{I}_{\text{emb/ion}}(z, z') \equiv \int d\bar{z} \Sigma_{\text{emb/ion}}(z, \bar{z}) G(\bar{z}, z') \quad (19)$$

is a convolution on the Keldysh contour between the embedding/ionization self-energy and the Green's function. The embedding self-energy is responsible for tunneling of electrons to/from the leads and reads [14, 47, 48]

$$\Sigma_{\text{emb}, ij}(z, \bar{z}) = \sum_{\alpha k} T_{i, \alpha k}(z) g_{\alpha k}(z, \bar{z}) T_{\alpha k, j}(\bar{z}), \quad (20)$$

where we allow for a time-dependent tunneling amplitude $T_{i, \alpha k}(z)$. The ionization self-energy is instead responsible for the photoionization of the system and reads [38, 40]

$$\Sigma_{\text{ion}, ij}(z, \bar{z}) = \sum_{\mu \in \mathcal{S}_{\text{ion}}} (\mathbf{E}(z) \cdot \mathbf{d}_{i\mu}) g_{\mu}(z, \bar{z}) (\mathbf{E}(\bar{z}) \cdot \mathbf{d}_{\mu j}). \quad (21)$$

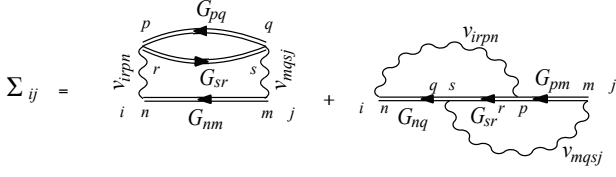


FIG. 2: Diagrammatic representation of the 2B self-energy. Wiggly lines denote the Coulomb interaction v .

Both self-energies are expressed in terms of a free-particle Green's function g . For the embedding self-energy $g_{\alpha k}$ is the solution of the equation of motion

$$\left[i \frac{d}{dz} - \Phi_{\alpha}(z) (\epsilon_{\alpha k} - V_{\alpha}(z)) \right] g_{\alpha k}(z, \bar{z}) = \delta(z, \bar{z}), \quad (22)$$

whereas for the ionization self-energy g_{μ} is the solution of the equation of motion

$$\left[i \frac{d}{dz} - \epsilon_{\mu} \right] g_{\mu}(z, \bar{z}) = \delta(z, \bar{z}). \quad (23)$$

All equations of motion, including Eq. (14), are solved with the appropriate Kubo-Martin-Schwinger boundary conditions [5].

There are two more terms to be discussed. The first term is the *collision* integral

$$\mathcal{I}_{\text{coll}}(z, z') \equiv \int d\bar{z} \Sigma(z, \bar{z}) G(\bar{z}, z'), \quad (24)$$

where the correlation self-energy $\Sigma = \Sigma[v, G]$ is a functional of the interaction v and the Green's function G . The exact Σ is the sum of all skeletonic self-energy diagrams with propagators G and interaction lines v [5]. In CHEERS this self-energy is implemented at the level of the second-Born (2B) approximation, i.e.,

$$\Sigma_{ij}(z, \bar{z}) = \sum_{mn pq sr} G_{mn}(z, \bar{z}) G_{pq}(z, \bar{z}) G_{sr}(\bar{z}, z) \times v_{irpm}(z) w_{nqsj}(\bar{z}). \quad (25)$$

In Fig. 2 we show the corresponding diagrammatic representation. We mention that the 2B approximation has been successfully applied to equilibrium spectral properties [49] and total energies [50] of molecular systems. Comparisons against numerically accurate real-time simulations of 1D systems [18, 51] and weakly correlated model nanostructures of different geometries [29, 30, 39, 52–56] indicate that the 2B approximation remains accurate even out of equilibrium.

The last term $\mathcal{I}_{\text{Auger}}$ can be written as in Eq. (24) but the self-energy contains all diagrams with at least one Auger interaction line v^A [57, 58]. If we are only interested in describing the Auger physics then we can approximate

$$\mathcal{I}_{\text{Auger}}(z, \bar{z}) = \int d\bar{z} \Sigma_{\text{Auger}}(z, \bar{z}) G(\bar{z}, z'), \quad (26)$$

where the Auger self-energy reads [41]

$$\begin{aligned} \Sigma_{\text{Auger}, ij}(z, \bar{z}) = & \sum_{mn pq} \sum_{\mu\nu \in \mathcal{S}_{\text{Auger}}} G_{mn}(z, \bar{z}) \\ & \times [G_{\mu\nu}(z, \bar{z}) G_{pq}(\bar{z}, z) (v_{iqm\mu}^A w_{nvpj}^A + v_{iq\mu m}^A w_{nvpj}^A) \\ & + G_{pq}(z, \bar{z}) G_{\mu\nu}(\bar{z}, z) v_{ivpm}^A w_{nq\mu j}^A]. \end{aligned} \quad (27)$$

This self-energy corresponds to the 2B approximation with interaction lines v^A and follows from the many-body identity $\Sigma = -iv^A G_2 G^{-1}$ where the two-particle Green's function G_2 describes a single Auger scattering. Notice that for strong valence-valence repulsive energies (typically well above 1 eV) it is crucial to replace the (first-order) single-scattering approximation to G_2 with the T -matrix approximation in the particle-particle channel [59, 60]. Currently, CHEERS does not contain implementations of the T -matrix approximation and hence it can only be used to study Auger decays in molecules (e.g., organic molecules) with fairly delocalized valence orbitals.

We observe that Σ_{Auger} depends on one Green's function with both indices in the continuum. Therefore Eq. (14) for G_{ij} can be solved only provided that we couple it to an equation for $G_{\mu\nu}$. To second order in v^A the equation of motion for $G_{\mu\nu}$ with $\mu, \nu \in \mathcal{S}_{\text{Auger}}$ is

$$\begin{aligned} \left[i \frac{d}{dz} - \epsilon_{\mu} \right] G_{\mu\nu}(z, z') = & \delta(z, z') + \sum_{\rho \in \mathcal{S}_{\text{Auger}}} \sum_{mn pq sr} \\ & \times \int d\bar{z} G_{mn}(z, \bar{z}) G_{pq}(z, \bar{z}) G_{sr}(\bar{z}, z) v_{\mu r p m}^A w_{n q s \rho}^A \\ & \times G_{\rho\nu}(\bar{z}, z) \end{aligned} \quad (28)$$

and it is linear in $G_{\mu\nu}$. An important consequence of this result is that if the Green's function of the initial state is block-diagonal in the indices i and μ , i.e., $G_{i\mu} = 0$, then it remains block diagonal.

Equations (14) and (28) form a coupled system of non-linear integro-differential equations and except for the 2B self-energy approximation no other approximations have been made. The full numerical solution of these equations requires to convert the contour-time G to real-time G 's, a procedure leading to the so-called Kadanoff-Baym equations (KBE). The numerical solution of the KBE is rather demanding, especially for large basis sets and many nonvanishing four-index Coulomb integrals. In the next section we discuss how the computational cost is drastically reduced by the GKBA.

B. GKBA equations

We rewrite the equation of motion (14) as

$$\begin{aligned} \left[i \frac{d}{dz} - h_{\text{HF}}(z) \right] G(z, z') = & \delta(z, z') \\ & + \int d\bar{z} \Sigma_{\text{tot}}(z, \bar{z}) G(\bar{z}, z'), \end{aligned} \quad (29)$$

with total self-energy

$$\Sigma_{\text{tot}} = \Sigma_{\text{ion}} + \Sigma_{\text{emb}} + \Sigma + \Sigma_{\text{Auger}}. \quad (30)$$

In Σ_{tot} only the last two terms are functionals of G . Choosing z and z' on different branches of the Keldysh contour we obtain the KBE for the lesser and greater Green's functions [4–6]

$$\left[i \frac{d}{dt} - h_{\text{HF}}(t) \right] G^{\lessgtr}(t, t') = \int d\bar{t} \Sigma_{\text{tot}}^{\text{R}}(t, \bar{t}) G^{\lessgtr}(\bar{t}, t') + \int d\bar{t} \Sigma_{\text{tot}}^{\lessgtr}(t, \bar{t}) G^{\text{A}}(\bar{t}, t'), \quad (31)$$

where, for any function F , the superscript R and A denotes the retarded and advanced components respectively:

$$F^{\text{R/A}}(t, t') = \pm \theta(\pm t \mp t') [F^>(t, t') - F^<(t, t')]. \quad (32)$$

Similarly, from the adjoint of Eq. (14) we find

$$G^{\lessgtr}(t, t') \left[\frac{1}{i} \frac{\overleftarrow{d}}{dt'} - h_{\text{HF}}(t') \right] = \int d\bar{t} G^{\text{R}}(t, \bar{t}) \Sigma_{\text{tot}}^{\lessgtr}(\bar{t}, t') + \int d\bar{t} G^{\lessgtr}(t, \bar{t}) \Sigma_{\text{tot}}^{\text{A}}(\bar{t}, t'). \quad (33)$$

Without any loss of generality we assume that the system is in equilibrium until a certain time $t_{\text{switch}} > 0$, hence $V_{\alpha}(t) = \mathbf{E}(t) = 0$ for $t < t_{\text{switch}}$. To obtain the *correlated* and *contacted* (to leads, if any) Green's function we solve Eqs. (31) and (33) with:

- initial condition $G^{\lessgtr}(0, 0)$ given by the HF (hence uncorrelated) lesser/greater Green's function of the uncontacted system
- self-energies calculated using a TD interaction $v(t) = s(t)v$ and tunneling amplitude $T(t) = s(t)T$ where $s(t)$ is a slow and smooth switching function between the times $t = 0$ and $t = t_{\text{switch}}$, typically $s(t) = \sin^2(\frac{\pi t}{2t_{\text{switch}}})$.

The time t_{switch} is therefore a convergence parameter to be chosen in such a way that the observables of interest are constant in the absence of external fields for times $t > t_{\text{switch}}$. This initial time-propagation serves to build up correlations in the initial state. Since $v = T = 0$ for times $t < 0$ the time integrals in the KBE run from 0 to ∞ , i.e., $\int d\bar{t} = \int_0^{\infty} d\bar{t}$.

Subtracting Eq. (33) from Eq. (31) and setting $t' = t$ we obtain the equation of motion for the one-particle density matrix $\rho_{ij} = -iG_{ij}^<(t, t)$

$$\dot{\rho}(t) + i[h_{\text{HF}}(t), \rho(t)] = -\mathcal{I}_{\text{tot}}(t) - \mathcal{I}_{\text{tot}}^{\dagger}(t), \quad (34)$$

where

$$\mathcal{I}_{\text{tot}}(t) = \int_0^t d\bar{t} [\Sigma_{\text{tot}}^>(t, \bar{t}) G^<(\bar{t}, t) - \Sigma_{\text{tot}}^<(t, \bar{t}) G^>(\bar{t}, t)]. \quad (35)$$

With similar steps, starting from Eq. (28) and its adjoint we can easily write down the equation of motion for the one-particle density matrix $f_{\mu\nu}(t) \equiv -iG_{\mu\nu}^<(t, t)$ with both indices $\mu, \nu \in \mathcal{S}_{\text{Auger}}$

$$\dot{f}_{\mu\nu}(t) + i(\epsilon_{\mu} - \epsilon_{\nu})f_{\mu\nu}(t) = -\mathcal{J}_{\mu\nu}(t) - \mathcal{J}_{\nu\mu}^*(t), \quad (36)$$

to be solved with boundary conditions $f_{\mu\nu}(0) = 0$ (no electrons in the continuum states at time $t = 0$). The right hand side of Eq. (36) describes the Auger scattering between localized electrons and continuum electrons and reads

$$\begin{aligned} \mathcal{J}_{\mu\nu}(t) = & \sum_{\rho \in \mathcal{S}_{\text{Auger}}} \sum_{mn pq sr} \int_0^t d\bar{t} v_{\mu r p m}^{\text{A}}(t) w_{n q s \rho}^{\text{A}}(\bar{t}) \\ & \times [G_{mn}^>(t, \bar{t}) G_{pq}^>(t, \bar{t}) G_{sr}^<(\bar{t}, t) G_{\rho\nu}^<(\bar{t}, t) \\ & - G_{mn}^<(t, \bar{t}) G_{pq}^<(t, \bar{t}) G_{sr}^>(\bar{t}, t) G_{\rho\nu}^>(\bar{t}, t)]. \end{aligned} \quad (37)$$

Due to the implicit (through Σ and Σ_{Auger}) and explicit dependence on G^{\lessgtr} evaluated at times $t \neq \bar{t}$, Eqs. (34) and (36) do not form a closed system of equations for ρ and f . To close the system we make the Generalized Kadanoff-Baym Ansatz [20] (GKBA)

$$-G_{ij}^<(t, t') = \sum_m [G_{im}^{\text{R}}(t, t') \rho_{mj}(t') - \rho_{im}(t) G_{mj}^{\text{A}}(t, t')], \quad (38a)$$

$$G_{ij}^>(t, t') = \sum_m [G_{im}^{\text{R}}(t, t') \bar{\rho}_{mj}(t') - \bar{\rho}_{im}(t) G_{mj}^{\text{A}}(t, t')], \quad (38b)$$

where $\bar{\rho} = 1 - \rho$. The functional form of the retarded/advanced propagator $G^{\text{R/A}} = G^{\text{R/A}}[\rho]$ will be discussed in Section V D. For the Green's function with both indices in the continuum, in addition to the GKBA we discard the off-diagonal matrix elements, i.e., we write

$$G_{\mu\nu} = \delta_{\mu\nu} G_{\mu}, \quad (39)$$

and approximate $G_{\mu}^{\text{R/A}} \simeq g_{\mu}^{\text{R/A}}$ where g_{μ} is the solution of Eq. (23). Hence

$$-G_{\mu}^<(t, t') = g_{\mu}^{\text{R}}(t, t') f_{\mu}(t') - f_{\mu}(t) g_{\mu}^{\text{A}}(t, t'), \quad (40a)$$

$$G_{\mu}^>(t, t') = g_{\mu}^{\text{R}}(t, t') \bar{f}_{\mu}(t') - \bar{f}_{\mu}(t) g_{\mu}^{\text{A}}(t, t'), \quad (40b)$$

where $\bar{f}_{\mu} = 1 - f_{\mu}$. With these approximations it is a matter of simple algebra to show that

$$\mathcal{J}_{\mu\nu}(t) = \int_0^t d\bar{t} [K_{\mu\nu}^>(t, \bar{t}) f_{\nu}(\bar{t}) + K_{\mu\nu}^<(t, \bar{t}) \bar{f}_{\nu}(\bar{t})] \quad (41)$$

where the kernel

$$\begin{aligned} K_{\mu\nu}^{\lessgtr}[\rho](t, \bar{t}) = & i \sum_{mn pq sr} v_{\mu r p m}^{\text{A}}(t) w_{n q s \nu}^{\text{A}}(\bar{t}) \\ & \times G_{mn}^{\lessgtr}(t, \bar{t}) G_{pq}^{\lessgtr}(t, \bar{t}) G_{sr}^{\lessgtr}(\bar{t}, t) e^{-i\epsilon_{\mu}(\bar{t}-t)} \end{aligned} \quad (42)$$

is a functional, through the GKBA, of ρ only.

With Eqs. (38) and (40) also the right hand side of Eq. (34) becomes a functional of ρ and f only. We thus obtain two coupled equations for the one-particle density matrix of an interacting system driven out of equilibrium by arbitrary biases $V_\alpha(t)$ and electric fields $\mathbf{E}(t)$ switched on at times $t > t_{\text{switch}}$:

$$\begin{cases} \dot{\rho} = -i[h_{\text{HF}}[\rho], \rho] - \mathcal{I}_{\text{tot}}[\rho, f] - \mathcal{I}_{\text{tot}}^\dagger[\rho, f] \\ \dot{f}_\mu = -\mathcal{J}_{\mu\mu}[\rho, f] - \mathcal{J}_{\mu\mu}^*[\rho, f] \end{cases} \quad (43)$$

These coupled equations govern the correlated electron dynamics in the NEGF+GKBA approach and are the equations solved by the CHEERS code. Both $\mathcal{I}(t)$ and $\mathcal{J}(t)$ depend on the density matrix at all previous times, thus introducing a memory dependence in the evolution. Time-dependent HF results are recovered by setting $\Sigma = \Sigma_{\text{Auger}} = \mathcal{J} = 0$. Notice that for $\Sigma_{\text{Auger}} = \mathcal{J} = 0$ the equations decouple and one needs to solve only the first equation since $f_\mu = 0$ is a solution.

The computational time to solve Eqs. (43) scales like $N_t^2 N_v$ where N_t is the number of time steps whereas $N_v = \max[N_{\text{bound}}^{\text{p}}, N_{\text{bound}}^{\text{q}} N_{\text{cont}}]$. Here N_{bound} is the dimension of the density matrix ρ , N_{cont} is the length of the vector f_μ and the powers $3 \leq \text{p} \leq 5$ and $2 \leq \text{q} \leq 4$ depend on how sparse the Coulomb tensors v_{ijmn} and v_{ijmn}^A are. In CHEERS the largest arrays are complex, double-precision, three-dimensional arrays of dimension $N_{\text{bound}} \times N_{\text{bound}} \times N_t$, and there are four such arrays. Thus, for a cluster with ~ 3 GB RAM per core CHEERS can perform simulations with $4 \times 16 \times N_{\text{bound}}^2 N_t < 3 \times 10^9$, i.e., $N_{\text{bound}}^2 N_t < 4.7 \times 10^7$.

IV. POST-PROCESSING: OBSERVABLE QUANTITIES

From the solution of Eqs. (43) we can calculate several quantities of physical interest. The most straightforward ones are the local density

$$n(\mathbf{r}, t) = \sum_{ij} \sum_{\sigma} \varphi_i^*(\mathbf{r}\sigma) \varphi_j(\mathbf{r}\sigma) \rho_{ji}(t), \quad (44)$$

spin density

$$\mathbf{s}(\mathbf{r}, t) = \sum_{ij} \sum_{\sigma\sigma'} \varphi_i^*(\mathbf{r}\sigma) \boldsymbol{\sigma}_{\sigma\sigma'} \varphi_j(\mathbf{r}\sigma') \rho_{ji}(t) \quad (45)$$

local paramagnetic current

$$\mathbf{j}(\mathbf{r}, t) = \frac{1}{2} \sum_{ij} \sum_{\sigma} \text{Im} [\varphi_i^*(\mathbf{r}\sigma) \nabla \varphi_j(\mathbf{r}\sigma) \rho_{ji}(t)], \quad (46)$$

and, more generally, any one-body observable. In Fig. 3 we show the snapshots of the density variation in the phenylalanine aminoacid induced by an ionizing attosecond XUV pulse [40], see Section VB for the implementation details.

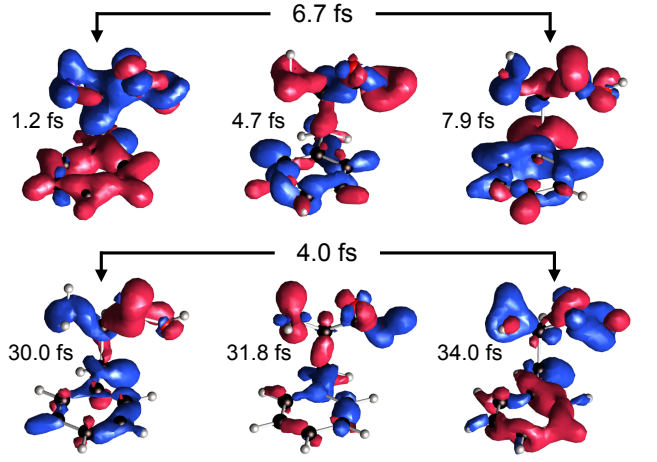


FIG. 3: Snapshots of the density variation in the phenylalanine aminoacid induced by an ionizing attosecond XUV pulse. The excess of hole density (blue) and electron density (red) refer to the density averaged over the full time simulation. Reprinted figure with permission from [40]. Copyright 2018 by the American Chemical Society.

Depending on the physical problem these basic quantities can be further manipulated to calculate typical experimental outcomes. In the following we discuss some of them.

A. Quantum Transport

In molecular electronics the Hamiltonian of the system describes a junction connecting two leads (a source and a drain) kept at a potential difference V . One is usually interested in the total current I flowing through a surface S perpendicular to the electron stream

$$I(t) = \int_S d^2r j_{\parallel}(\mathbf{r}, t), \quad (47)$$

with j_{\parallel} the longitudinal component of \mathbf{j} , see Eq. (46). For a DC bias $I(t)$ attains a steady value as $t \rightarrow \infty$ and this value can be used to calculate the $I - V$ characteristics or the differential conductance $\mathcal{G} = dI/dV$. Of course, the full time-evolution provides other useful information. The characteristic time to reach a steady state and the frequencies of the transient oscillations are just two examples. Controlling these properties is crucial to engineer ultrafast molecular devices.

Time-dependent potential differences $V(t)$ do not bring additional complications nor an increased computational effort. We can, for instance, superimpose an AC voltage of frequency Ω to a DC voltage, i.e., $V(t) = V_{\text{DC}} + V_{\text{AC}} \sin(\Omega t)$, and calculate the averaged current as well as its Fourier coefficients as functions of V_{DC} , V_{AC} and Ω . In addition to provide an alternative to Floquet schemes [61], working in the time domain is particularly

advantageous to deal with systems perturbed by multichromatic drivings. This is the case of, e.g., AC transport with superconducting leads [62] or optical spectra of junctions under AC voltages [46].

The current $I(t)$ can be evaluated either at an interface passing through the junction, in accordance with Eq. (47), or at the interface with the α lead through the Meir-Wingreen formula [47, 48]

$$I_\alpha(t) = 4\text{Re} \int_0^t d\bar{t} \text{Tr} [\Sigma_\alpha^>(t, \bar{t})G^<(\bar{t}, t) - \Sigma_\alpha^<(t, \bar{t})G^>(\bar{t}, t)] \quad (48)$$

where Σ_α is the α -th contribution to the embedding self-energy of Eq. (20) and G^\lessgtr are calculated from ρ through the GKBA. In Ref. 21 we showed that the GKBA results for the current at the interfaces are in excellent agreement with the full KBE results provided that the bias difference is much smaller than the bandwidth of the leads. We mention that an improved version of the GKBA has been recently proposed to deal with nontrivial spectral structures of the leads density-of-states [63], thus widening the potential applications of the GKBA in quantum transport.

The energy current $J_\alpha(t)$, defined as the rate of change of the energy of lead α , can be calculated similarly to the charge current in Eq. (49). It is a matter of simple algebra to show that [43]

$$J_\alpha(t) = 4\text{Im} \int_0^t d\bar{t} \text{Tr} [\dot{\Sigma}_\alpha^>(t, \bar{t})G^<(\bar{t}, t) - \dot{\Sigma}_\alpha^<(t, \bar{t})G^>(\bar{t}, t)] \quad (49)$$

where $\dot{\Sigma}_\alpha^\lessgtr(t, \bar{t}) \equiv \frac{d}{dt} \Sigma_\alpha^\lessgtr(t, \bar{t})$.

B. Transient Photoabsorption Spectra

In a transient photoabsorption spectrum the system is driven out of equilibrium by a strong laser pulse (the pump) and successively the intensity per unit frequency of the transmitted light of a second weak pulse (the probe) is measured. The resulting transient spectrum depends on the shape and duration of the pump and probe pulses as well as from the delay τ between these pulses. It is therefore clear that the theoretical calculation of a transient spectrum calls for a time-dependent approach.

Let $\langle \delta \mathbf{d}(t, \tau) \rangle$ be the change of the dipole moment of the pump-driven system induced by an electric probe field $\mathbf{e}(t)$ impinging the system with a delay τ with respect to the pump. Then the transient spectrum is given by

$$\mathfrak{S}(\omega, \tau) = -2\text{Im} [\omega \tilde{\mathbf{e}}^*(\omega) \cdot \langle \delta \tilde{\mathbf{d}}(\omega, \tau) \rangle] \quad (50)$$

where we have used the convention that quantities with a tilde denote the Fourier transform of the corresponding time-dependent quantities.

The dipole moment of the system can easily be calculated from the one-particle density matrix as

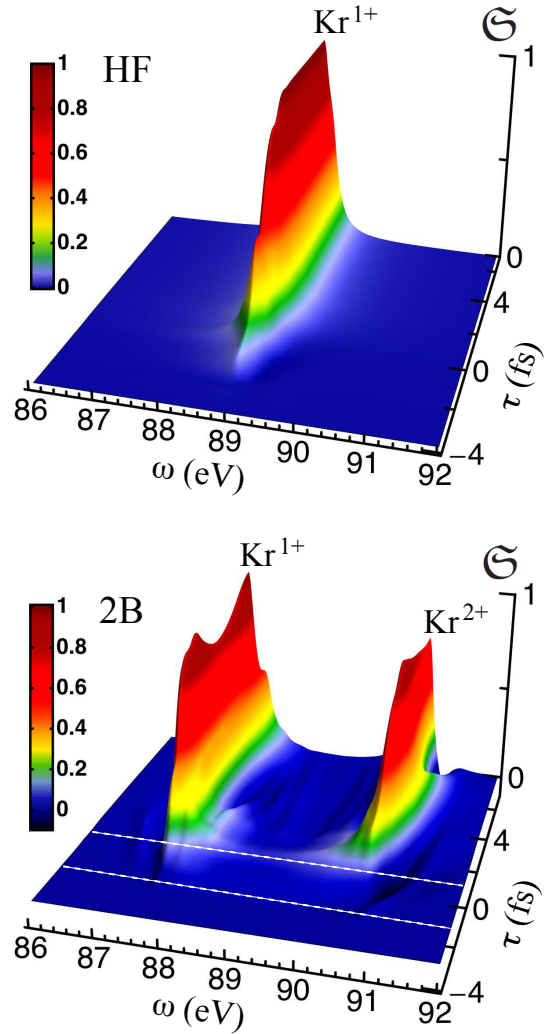


FIG. 4: Transient photoabsorption spectrum (normalized to the maximum height) of a krypton gas in the HF (top panel) and 2B (bottom panel) approximation. Reprinted figure with permission from [38]. Copyright 2015 by the American Physical Society.

$\langle \mathbf{d}(t) \rangle = \sum_{ij} \mathbf{d}_{ij} \rho_{ji}(t)$. The probe-induced dipole moment $\langle \delta \mathbf{d}(t, \tau) \rangle$ is therefore the difference between the dipole moment generated by a simulation with pump and probe and the dipole moment generated by a simulation with only the pump. We observe that the pump pulse can either bring the system in an excited state of bound electrons or generate a multiply ionized system through the ionization integral \mathcal{I}_{ion} . In the latter case the transient spectrum reveals features about the initial dynamics of the expelled photoelectrons [64]. In Fig. 4 we display HF (top) and correlated (bottom) calculations of the transient spectrum of a gas of Kr atoms initially ionized by few-cycle NIR pump and subsequently probed by an attosecond XUV pulse at different delays τ [38], see Section V A for the implementation details. In HF no sign

of multiple ionization is visible. On the contrary, the correlated 2B results clearly show the absorption line of Kr^{2+} ions raising up a few femtosecond later than the absorption line of Kr^{1+} .

C. Transient Photocurrent and Auger Current

In the absence of leads (closed system) the total electric current flowing out of the system, i.e., in the continuum states, can be calculated from the rate of change of the total number of particles in the system

$$I_{\text{ion}}(t) = \frac{dN(t)}{dt} = \frac{d}{dt} \text{Tr}[\rho(t)]. \quad (51)$$

If we are interested in resolving the photocurrent according to the energy of the photoelectrons (photoemission spectrum) we should include explicitly the continuum states $\mu \in \mathcal{S}_{\text{ion}}$ in the simulation (instead of using Σ_{ion}). We would then get a third equation for the occupations f_{μ} with $\mu \in \mathcal{S}_{\text{ion}}$ coupled to Eqs. (43). Of course this procedure is feasible only provided that the energy window of the photoelectrons is not too wide and that the number of μ states for the required energy resolution is not too large. At present the explicit inclusion of photoelectron states has been tested only in one-dimensional model systems [41].

The Auger self-energy accounts for processes where two valence electrons scatter and, after the scattering, end up in a core state and in a continuum state. The rate of growth of the occupation of the continuum state $\mu \in \mathcal{S}_{\text{Auger}}$ defines the Auger current

$$I_{\text{Auger}}(t) = \frac{d}{dt} f_{\mu}(t). \quad (52)$$

Through knowledge of ρ_{ij} and f_{μ} we can follow in real time the Auger scattering and extract useful information about the Auger process, e.g., core relaxation time, shape of the outgoing density wavepacket, rearrangement of the core-excited system, etc [41].

V. IMPLEMENTATION DETAILS

From Eqs. (43) and the definition of the various quantities therein we find useful to split the input parameters into five different groups

- *System*: matrix elements h_{ij}^{eq} , \mathbf{d}_{ij} and Coulomb integrals v_{ijmn}
- *Ionization*: matrix elements $\mathbf{d}_{i\mu}$ and energies ϵ_{μ} with $\mu \in \mathcal{S}_{\text{ion}}$
- *Auger*: matrix elements $\mathbf{d}_{i\mu}$, energies ϵ_{μ} and Coulomb integrals $v_{ijm\mu}^A$ with $\mu \in \mathcal{S}_{\text{Auger}}$
- *Leads*: tunneling amplitudes $T_{i,\alpha k}$ and energies $\epsilon_{\alpha k}$

- *External fields*: electric field $\mathbf{E}(t)$, bias $V_{\alpha}(t)$ and temperature $T_{\alpha}(t)$.

Currently, real-time simulations in the presence of leads (open systems) are performed only for model Hamiltonians. Here, the input parameters are set manually and can be varied at will. Real-time simulations based on first-principles input parameters are possible for closed systems ($\Sigma_{\text{emb}} = 0$) like atoms and molecules in external laser fields. CHEERS handles the input parameters in different way depending on the nature of the single-particle basis set. In the following two subsections we describe how CHEERS processes the input generated in a basis of localized orbitals like, e.g., Slater Type Orbitals (STO) or Gaussian Type Orbitals (GTO), and in a basis of Kohn-Sham orbitals. In all cases the first step of CHEERS is to obtain the information contained in *System*, *Ionization*, *Auger* and *Leads*. With this information CHEERS calculates all self-energies and then passes them to the time-propagation routine, see blue arrows in Fig. 5.

As illustrated in the left red box of Fig. 5 the time-propagation routine needs also other information. Two main flags specify the type of evolution. One flag establishes the level of correlation: it can be either a HF evolution – with the extra option of using the HF Hamiltonian $h_{\text{HF}}[\rho(t_{\text{switch}})](t)$ with frozen ρ instead of $h_{\text{HF}}[\rho(t)](t)$ – or a correlated 2B evolution. Another flag sets which propagator $G^{\text{R}}[\rho]$ is used in the GKBA, see subsection VD for the possible choices. Prior to the time evolution we also specify a few convergence parameters. The most important ones are the time-step, the switching time t_{switch} for the correlation build-up and the number of predictor correctors for each time step. Finally, we specify the driving fields in the input *External fields*. There are no restrictions on the time-dependent functions $\mathbf{E}(t)$, $V_{\alpha}(t)$ and $T_{\alpha}(t)$, and the computational effort does not depend on the choice of these functions. During the time stepping the density matrix ρ_{ij} and f_{μ} are either saved or processed to generate the output described in Section IV.

A. Localized basis

For a description in terms of N single-particle localized states $\{|i\rangle\}$ like, e.g., the STO or GTO states, CHEERS needs the matrix elements of the equilibrium Hamiltonian h_{ij}^{eq} , dipole vector \mathbf{d}_{ij} , overlap matrix $S_{ij} = \langle i|j\rangle$ and Coulomb integrals v_{ijmn} . The first step of CHEERS is to orthonormalize the basis according to $|i\rangle \rightarrow \sum_m |m\rangle S_{mi}^{-1/2}$, calculate h_{ij}^{eq} , \mathbf{d}_{ij} and v_{ijmn} in the new orthonormal basis and run a HF self-consistent calculation. The second step is to calculate h_{ij}^{eq} , \mathbf{d}_{ij} and v_{ijmn} in the HF basis which, by definition, diagonalizes the HF Hamiltonian $h_{\text{HF},ij} = \epsilon_i^{\text{HF}} \delta_{ij}$. This is done only for HF states with energy $\Lambda_{\text{min}} < \epsilon_i^{\text{HF}} < \Lambda_{\text{max}}$ where Λ_{min} and Λ_{max} are two convergence cutoff parameters. Of course if Λ_{min} is smaller than the minimum HF eigen-

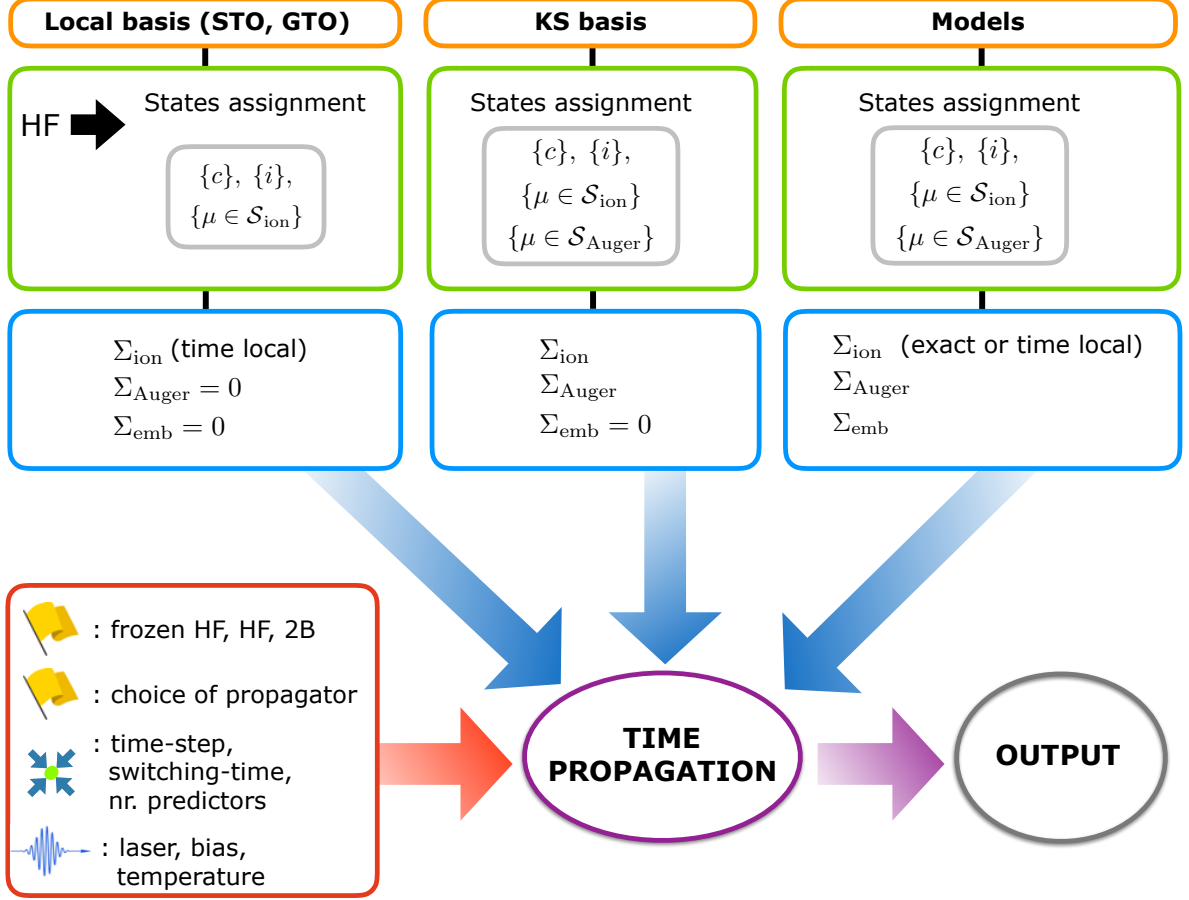


FIG. 5: Architecture of CHEERS. The input contained in *System*, *Ionization*, *Auger* and *Leads* can be either generated from first-principles calculations in a localized basis (left) or KS basis (middle) or, alternatively, it can be set manually for model system calculations (right). The level of correlation, type of propagator, convergence parameters and the input of *External fields* is given in the red box (bottom right). During the time propagation the density matrix is either saved or processed to generate the output of interest.

value and Λ_{max} is larger than the maximum HF eigenvalue then all N HF states are included. On the contrary, states $i = c$ of energy $\epsilon_c^{\text{HF}} < \Lambda_{\text{min}}$ are treated as core states, i.e., $\rho_{cc'} = \delta_{cc'}$. Then CHEERS calculates only v_{iccj} and v_{icjc} and adds to the equilibrium Hamiltonian the HF potential generated by the frozen core (fc) electrons:

$$h_{ij}^{\text{eq}} \rightarrow h_{ij}^{\text{eq+fc}} = h_{ij}^{\text{eq}} + \sum_c (v_{iccj} - v_{icjc}). \quad (53)$$

The HF states $i = \mu$ with energy $\epsilon_\mu^{\text{HF}} > \Lambda_{\text{max}}$ are treated as noninteracting and considered as states of the continuum. Accordingly, CHEERS calculates only the dipole matrix elements $\mathbf{d}_{i\mu}$ later used to construct the ionization self-energy of Eq. (21). The separation of the HF states is illustrated in the left green box of Fig. 5.

After this preliminary treatment the size of the one-particle density matrix ρ in Eq. (34) becomes $N_{\text{bound}} = N - N_c - N_{\text{ion}}$, where N_c is the number of HF core states and N_{ion} is the number of μ -states. The STO or GTO description of the continuum is, in general, too poor for

simulating Auger scattering processes which are therefore not included, see left blue box of Fig. 5. This means that for a localized basis CHEERS solves only the first of Eqs. (43). For problems involving Auger scattering see next Section.

The μ -states of the localized basis are used to construct an approximate ionization self-energy, thus accounting for possible photoelectrons due to external laser fields. Of course, if the expected energy range of the photoelectrons is not covered by the ϵ_μ^{HF} then the ionization rate is severely underestimated. Meaningful real-time simulations do therefore require that the laser frequency is at least smaller than $\max\{\epsilon_\mu^{\text{HF}}\} - 2\pi/T$ where T is the duration of the ionizing pulse.

Let us discuss the ionization self-energy. In general the STO or GTO basis returns only a few continuum states; consequently, a photoelectron would be soon reflected back. This difficulty can be overcome provided that the ionizing laser pulse is well centered around some frequency ω_P . From Eq. (21) the lesser part of Σ_{ion} van-

ishes whereas the greater part is given by

$$\Sigma_{\text{ion}}^>(t, t') = \sum_{ab} E_a(t) \sigma^{ab}(t - t') E_b(t'), \quad (54)$$

where E_a is the a -th component of the electric field $\mathbf{E} = (E_x, E_y, E_z)$ and the tensor

$$\sigma_{ij}^{ab}(t - t') \equiv -i \sum_{\mu \in \mathcal{S}_{\text{ion}}} d_{i\mu}^a e^{-i\epsilon_\mu^{\text{HF}}(t-t')} d_{\mu j}^b, \quad (55)$$

depends exclusively on the matrix elements of the components d^a of the dipole moment $\mathbf{d} = (d^x, d^y, d^z)$. The Fourier transform of σ_{ij}^{ab} reads

$$\begin{aligned} \tilde{\sigma}_{ij}^{ab}(\omega) &= -2\pi i \sum_{\mu \in \mathcal{S}_{\text{ion}}} d_{i\mu}^a \delta(\omega - \epsilon_\mu^{\text{HF}}) d_{\mu j}^b \\ &\approx 2i \sum_{\mu \in \mathcal{S}_{\text{ion}}} d_{i\mu}^a \text{Im} \left[\frac{1}{\omega - \epsilon_\mu^{\text{HF}} + i\eta} \right] d_{\mu j}^b, \end{aligned} \quad (56)$$

where η is a positive constant of the order of the level spacing of the μ -states. Since $\mathbf{E}(t)$ oscillates at the frequency ω_P the ionization self-energy is dominated by those terms in $\sigma(t - t')$ that oscillate at energy $\epsilon_\mu^{\text{HF}} \simeq \omega_P$. We do therefore implement a frequency-independent approximation $\tilde{\sigma}_{ij}^{ab}(\omega) \approx \tilde{\sigma}_{ij}^{ab}(\omega_P)$, which in real time implies $\sigma_{ij}^{ab}(t - t') = \tilde{\sigma}_{ij}^{ab}(\omega_P) \delta(t - t')$. Substituting this result into Eq. (54) we get

$$\Sigma_{\text{ion}}^>(t, t') = -i\delta(t - t') \Gamma_{\text{ion}}(t), \quad (57)$$

where

$$\Gamma_{\text{ion},ij}(t) = i \sum_{ab} E_a(t) \tilde{\sigma}_{ij}^{ab}(\omega_P) E_b(t) \quad (58)$$

is a self-adjoint positive-definite matrix for all times t . Thus, the approximate Σ_{ion} is a local function of time as indicated in the left blue box of Fig. 5.

The transient photoabsorption spectrum of the Kr gas in Fig. 4 [38] has been calculated using the 66 STO from Ref. [65] as basis, generating the input in *System* and *Ionization* with the SMILES package [66, 67], freezing all electrons below the 3d shell and constructing Σ_{ion} with the HF states of positive energy.

B. Kohn-Sham basis

In general the finite system of interest can be described in terms of a single-particle basis formed by core states and a rest. The rest is a set of *active* states, i.e., states with a population different from 0 or 1 because of dynamical correlations or thermal fluctuations or external fields. Let \mathcal{C} and \mathcal{A} be the set of core states and active states respectively. Since, by definition, for $i \in \mathcal{C}$ every physically relevant many-body state is an eigenstate of $\hat{c}_i^\dagger \hat{c}_i$ with eigenvalue 1, we can work in the truncated

Hilbert space of many-body states having the core states entirely filled. In this truncated Hilbert space the density matrix ρ satisfies again Eq. (43) but with a different HF Hamiltonian h_{HF} .

To determine the HF Hamiltonian for the “active” electrons let us split the contributions (core and active) to the Hartree and exchange potential

$$V_{\text{H},ij}^{\mathcal{S}}[\rho] \equiv \sum_{mn \in \mathcal{S}} v_{imnj} \rho_{nm}, \quad ij \in \mathcal{A} \quad (59)$$

$$V_{\text{x},ij}^{\mathcal{S}}[\rho] \equiv - \sum_{mn \in \mathcal{S}} v_{imjn} \rho_{nm}, \quad ij \in \mathcal{A}. \quad (60)$$

where $\mathcal{S} = \mathcal{C}, \mathcal{A}$ and the indices i, j run in the active set \mathcal{A} . Taking into account that $\rho_{nm} = \delta_{nm}$ for $n, m \in \mathcal{C}$ the equilibrium HF Hamiltonian in Eq. (15) can be rewritten as

$$h_{\text{HF}}[\rho] = h^{\text{eq+fc}} + V_{\text{H}}^{\mathcal{A}}[\rho] + V_{\text{x}}^{\mathcal{A}}[\rho], \quad (61)$$

where

$$h^{\text{eq+fc}} = h^{\text{eq}} + V_{\text{H}}^{\mathcal{C}} + V_{\text{x}}^{\mathcal{C}} \quad (62)$$

is the one-particle Hamiltonian plus the HF potential generated by the frozen core electrons.

So far we have not yet specified the single-particle basis. We here consider the case of a Kohn-Sham (KS) basis. Hence we assume that electrons in the KS core orbitals remain frozen and do not participate to the dynamics. The equilibrium KS one-particle density matrix in the KS basis reads $\rho_{\text{KS},nm} = \delta_{nm}$ and the corresponding equilibrium KS Hamiltonian is diagonal and reads

$$h_{\text{KS}} = h^{\text{eq}} + V_{\text{H}}^{\mathcal{C}} + V_{\text{xc}} + V_{\text{H}}^{\mathcal{A}}[\rho_{\text{KS}}], \quad (63)$$

where V_{xc} is the exchange-correlation potential of Density Functional Theory (DFT). In general, $V_{\text{H}}^{\mathcal{C}} + V_{\text{xc}}$ is given by the sum of the pseudopotential and the xc potential generated by the active electrons. A comparison with Eq. (61) allows us to express $h^{\text{eq+fc}}$ in terms of the KS Hamiltonian according to

$$h^{\text{eq+fc}} = h_{\text{KS}} - V_{\text{xc}} - V_{\text{H}}^{\mathcal{A}}[\rho_{\text{KS}}] + V_{\text{x}}^{\mathcal{C}}. \quad (64)$$

Depending on the system and laser pulse properties the electrons in states with $\epsilon_i^{\text{KS}} < \Lambda_{\text{max}}$ are explicitly propagated through ρ , whereas states $i = \mu$ with energy $\epsilon_\mu^{\text{KS}} > \Lambda_{\text{max}}$ are either assigned to \mathcal{S}_{ion} or $\mathcal{S}_{\text{Auger}}$, see middle green box in Fig. 5 (here Λ_{max} is a convergence parameter). Thus, CHEERS needs the KS eigenvalues ϵ_i^{KS} (needed to construct the KS Hamiltonian $h_{\text{KS},ij} = \delta_{ij} \epsilon_i^{\text{KS}}$), the matrix elements $V_{\text{xc},ij}$, \mathbf{d}_{ij} and the Coulomb integrals v_{ijmn} (needed to evaluate the Hartree potential $V_{\text{H}}^{\mathcal{A}}[\rho_{\text{KS}}]$ generated by the active KS electrons as well as the functionals $V_{\text{H}}^{\mathcal{A}}$, $V_{\text{x}}^{\mathcal{A}}$ and Σ), the dipole matrix elements $\mathbf{d}_{i\mu}$ and KS energies ϵ_μ^{KS} with $\mu \in \mathcal{S}_{\text{ion}}$ (needed to calculate the ionization self-energy Σ_{ion}) and

the Coulomb integrals $v_{ijm\mu}^A$ and KS energies ϵ_μ^{KS} with $\mu \in \mathcal{S}_{\text{Auger}}$ (needed to calculate the Auger self-energy Σ_{Auger} and the kernel K), see middle blue box in Fig. 5. This input contains the necessary quantities to construct the functionals \mathcal{I}_{tot} and \mathcal{J} , see Eqs. (43), as well as the HF Hamiltonian in Eq. (64). In fact, the only remaining unknown is $V_x^{\mathcal{C}}$ which, however, is usually small and can be neglected. Of course, a non-negligible $V_x^{\mathcal{C}}$ does not introduce extra complications for the CHEERS simulations. One could estimate this quantity by performing an all-electron KS calculation without pseudopotentials.

The snapshots of the density variation of the phenylalanine aminoacid in Fig. 3 [40] has been calculated by performing a DFT calculation with the Quantum Espresso package [68] using norm-conserving Troullier-Martins pseudopotentials [69] and the PBE approximation [70] for V_{xc} . The resulting KS states have then been used to extract the matrix elements $V_{\text{xc},ij}$, \mathbf{d}_{ij} , $\mathbf{d}_{i\mu}$ and the Coulomb integrals v_{ijmn} using the Yambo code [71] (no Auger scattering was included since only valence electrons are ionized by the XUV pulse).

C. An application to Argon: STO versus KS basis

As long as the single-particle basis is complete the CHEERS results are independent of the basis. The purpose of this Section is to illustrate this fact with an example. We consider the Argon atom and monitor the time-evolution of the occupations of the HF orbitals after a sudden ionization. The calculations are performed in two different basis:

(i) the STO basis of Clementi-Roetti [72] consisting of 32 basis functions. The input has been obtained with the SMILES package [66, 67] and no electron has been frozen (hence electrons of the K and L shells participate to the dynamics).

(ii) the KS basis obtained by performing a DFT calculation with the Octopus code [73] using norm-conserving Troullier-Martins pseudopotentials [69] and the Perdew-Zunger xc functional [74].

In both cases we start from an initial density matrix corresponding to the state of the system just after an ionizing laser pulse has passed through the atom. Typical attosecond pulses remove less than 1% of charge from the neutral system. Here, in order to highlight the effects of correlations, we consider an initial density matrix $\rho_{a\sigma,b\sigma'}(0) = \delta_{\sigma\sigma'}\rho_{a,b}(0)$ where $\rho(0) = \rho^{\text{eq}} - \delta\rho$ and $\delta\rho$ in HF basis reads $\delta\rho_{3s,3s} = 0.1$, $\delta\rho_{3p_x,3p_x} = 0.1$ and $\delta\rho_{3s,3p_x} = \delta\rho_{3p_x,3s} = -0.1$. This corresponds to remove 0.2 electrons of spin up and down.

In Fig. 6 we compare the results in the two different basis as obtained by running CHEERS in the HF and 2B approximation. In HF the time-evolution is dominated by $3s \leftrightarrow 3p_x$ transitions and resembles the evolution of a noninteracting two-level system, in agreement with the fact that the HF theory is a single-particle theory and the system is weakly correlated. On the contrary, the corre-

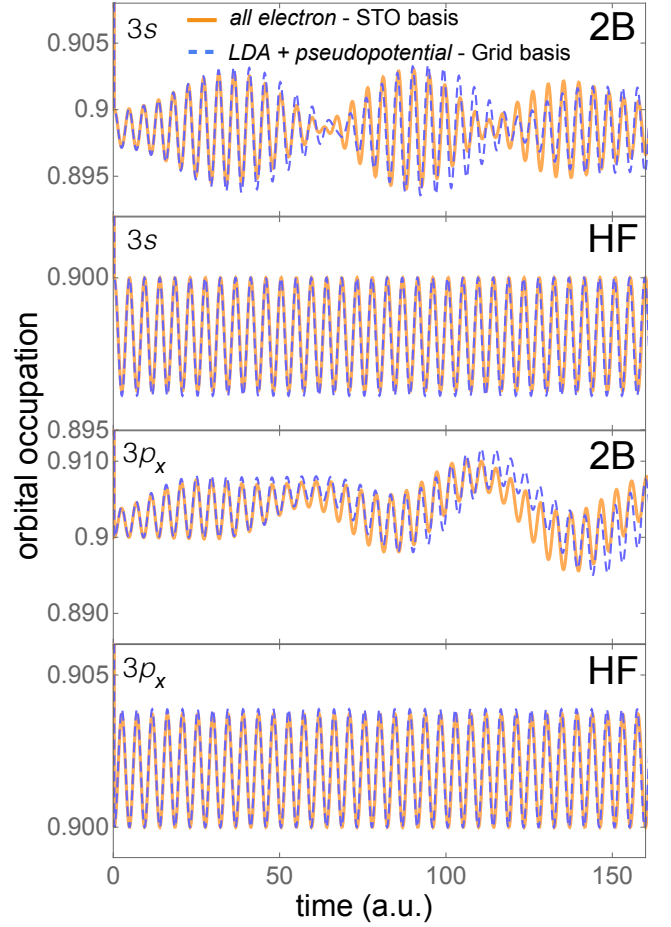


FIG. 6: Time-dependent evolution of the occupations of the equilibrium HF orbitals $3s$ and $3p_x$ after a sudden ionization, as described in the main text. The calculations have been performed using the HF (second and fourth panels) and 2B (first and third panels) approximation.

lated 2B evolution highlights the occurrence of scatterings involving $3p_y$ and $3p_z$ electrons. In fact, the initial density matrix describes a mixture of charge neutral Ar and multiply ionized Ar^{n+} with $n = 1, \dots, 6$. In the considered Hilbert space Ar^+ can only give rise to the oscillation corresponding to the transition $3s \leftrightarrow 3p$ while Ar^{2+} can only give rise to oscillations corresponding to the transitions $3s^2 \leftrightarrow 3s3p$ and $3s3p \leftrightarrow 3p^2$. These are degenerate in HF although in reality they should not. 2B correctly removes the degeneracy giving rise to the observed beating. Doubly and multiply ionized Ar atoms contributes less since we have removed only 40% of an electron. Aside from the physical interpretation of the results, the figure clearly show that the outcomes stemming from using two different basis (and procedures) are in a fairly good agreement.

D. Retarded propagator

In this section we discuss the possible choices of the retarded Green's function. The exact equation of motion for G^R reads

$$\left[i \frac{d}{dt} - h_{\text{HF}}(t) \right] G^R(t, t') = \delta(t, t') + \int d\bar{t} \Sigma_{\text{tot}}^R(t, \bar{t}) G^R(\bar{t}, t') \quad (65)$$

to be solved with boundary condition $G^R(t, t^+) = -i$. The lowest order (in the Coulomb integrals) approximation for G^R is obtained by setting $\Sigma_{\text{tot}}^R = 0$. In this case we get the HF propagator

$$G^R(t, t') = -i\theta(t - t') T e^{-i \int_{t'}^t d\bar{t} h_{\text{HF}}(\bar{t})}. \quad (66)$$

In CHEERS all approximations to G^R have the form of Eq. (66) where h_{HF} is replaced by some quasi-particle Hamiltonian $h_{\text{qp}} = h_{\text{HF}} + \Delta$. For $\Delta = 0$ we recover the HF propagator. The advantage of approximations like in Eq. (66) is that for small δt

$$G^R(t + \delta t, t') \simeq e^{-i \frac{h_{\text{qp}}(t + \delta t) + h_{\text{qp}}(t)}{2} \delta t} G^R(t, t') \quad (67)$$

and hence the calculation of $G^R(t, t')$ for all $t' < t$ scales linearly in t . Consequently, the overall scaling remains quadratic with the maximum propagation time.

The presence of a continuum due to leads and/or photoelectron states can be partially taken into account by approximating

$$\Sigma_{\text{emb/ion}}^R(t, t') \simeq -(i/2)\delta(t - t')\Gamma_{\text{emb/ion}}(t) \quad (68)$$

where Γ_{ion} is defined in Eq. (58) whereas

$$\Gamma_{\text{emb}, ij} = -2 \sum_{k\alpha} T_{i, \alpha k} \text{Im} \left[\frac{1}{-\epsilon_{\alpha k} + i\eta} \right] T_{\alpha k, j}, \quad (69)$$

see Ref. [21]. Setting $\Sigma^{\text{tot}} = \Sigma_{\text{emb}}^R + \Sigma_{\text{ion}}^R$ in Eq. (65) one finds $\Delta = -(i/2)(\Gamma_{\text{emb}} + \Gamma_{\text{ion}})$.

Correlation effects in the propagator can be taken into account by making the approximation [21]

$$\begin{aligned} \int d\bar{t} \Sigma^R(t, \bar{t}) G^R(\bar{t}, t') &\simeq \left[\int d\bar{t} \Sigma^R(t, \bar{t}) \right] G^R(t, t') \\ &\equiv \tilde{\Sigma}(t) G^R(t, t'), \end{aligned} \quad (70)$$

which amounts to add $\tilde{\Sigma}$ to h_{HF} . We evaluate $\tilde{\Sigma}(t)$ in Eq. (70) using the GKBA and the adiabatic propagator

$$\tilde{G}_{\text{ad}}^R(t, t') = \int \frac{d\omega}{2\pi} \frac{e^{-i\omega(t-t')}}{\omega - h_{\text{qp}}(t) + i\eta}. \quad (71)$$

In this way we generate a self-consistent equation for $\tilde{\Sigma}(t) = \tilde{\Sigma}[\rho(t), h_{\text{qp}}(t)]$. In practice at the n -th time step we determine $\rho(t_{n+1})$ from Eq. (43), then calculate $h_{\text{qp}}(t_{n+1})$ using $\tilde{\Sigma}(t_{n+1}) = \tilde{\Sigma}(t_n)$, hence $\tilde{G}^R(t_{n+1}, t')$ and finally the new $\tilde{\Sigma}(t_{n+1})$. This procedure is repeated

a few times to achieve convergence. We point out that propagator used in the evaluation of \mathcal{I}_{tot} is G^R and not the adiabatic \tilde{G}^R . The latter is only an auxiliary quantity to evaluate $\tilde{\Sigma}(t)$.

In CHEERS the quasi-particle Hamiltonian used for G^R reads

$$h_{\text{qp}} = h_{\text{HF}} - (i/2)(\alpha_{\text{emb}}\Gamma_{\text{emb}} + \alpha_{\text{ion}}\Gamma_{\text{ion}}) + \alpha_{\text{ad}}\tilde{\Sigma}, \quad (72)$$

where the parameters $\alpha_{\text{emb}}, \alpha_{\text{ion}}, \alpha_{\text{ad}}$ can be set to either 0 or 1.

VI. CONCLUDING REMARKS

To the best of our knowledge, CHEERS is currently the only code which combines ab initio methods with NEGF to calculate the nonequilibrium dynamics of molecular systems. CHEERS has already been used to study the charge dynamics of molecular junctions [21], time-resolved photoabsorption of noble gas atoms [38, 75], charge separation in donor-acceptor complexes [39], charge migration in organic molecules [40] and time-resolved Auger decays [41]. The code handles inputs obtained in any basis and can perform all-electrons as well as pseudopotential calculations.

Currently, dynamical correlations are included at the level of the 2B approximation for the self-energy, although the scaling of the computational cost remains identical using a statically screened electron-electron interaction for the exchange and second-order diagrams [39]. Self-energy approximations like GW or T-matrix would restore the cubic KBE scaling with the number of time steps unless a GKBA for W or T is provided, an advance which would be of utmost theoretical and computational value.

So far CHEERS simulations involving photoionization processes have been performed using the KS continuum states generated either by the Quantum Espresso code [68] (planewave basis) or by the Octopus code [73] (grid basis). Another promising alternative consists in using a B-spline basis [76, 77]. In a recent work, the B-spline basis has been combined with the algebraic diagrammatic construction method to calculate the attosecond pump-probe spectrum of carbon dioxide [78].

Another limitation of CHEERS is that the nuclear positions are kept fixed during the time evolution. Work to include harmonic effects through a Fan self-energy [79] evaluated with ab-initio frequencies and electron-nuclear couplings is in progress. We are also planning to implement the semiclassical Ehrenfest dynamics which requires to calculate all one- and two-electron integrals along the nuclear trajectory. This extension of CHEERS is especially relevant to access the subpicosecond timescale (10÷100 fs) typical of charge transfer and charge separation processes.

Acknowledgements

We acknowledge inspiring and insightful discussions with Emil Böstrom, Fabio Covito, Daniel Karlsson, Simone Latini, Andrea Marini, Yaroslav Pavlyukh, Angel Rubio, Davide Sangalli, Anna-Maija Uimonen, Robert van Leeuwen and Claudio Verdozzi. We also acknowledge EC funding through the RISE Co-ExAN (Grant

No. GA644076). E.P. also acknowledges funding from the European Union project MaX Materials design at the eXascale H2020-EINFRA-2015-1, Grant Agreement No. 676598 and Nanoscience Foundries and Fine Analysis-Europe H2020-INFRAIA-2014-2015, Grant Agreement No. 654360. G.S. also acknowledges Tor Vergata University for financial support through the Mission Sustainability Project 2DUTOPI.

-
- [1] F. Krausz and M. Ivanov, *Rev. Mod. Phys.* **81**, 163 (2009), URL <https://link.aps.org/doi/10.1103/RevModPhys.81.163>.
 - [2] L. Gallmann, C. Cirelli, and U. Keller, *Annual Review of Physical Chemistry* **63**, 447 (2012), URL <https://doi.org/10.1146/annurev-physchem-032511-143702>.
 - [3] M. Nisoli, P. Decleva, F. Calegari, A. Palacios, and F. Martín, *Chemical Reviews* **117**, 10760 (2017), pMID: 28488433, URL <http://dx.doi.org/10.1021/acs.chemrev.6b00453>.
 - [4] P. Danielewicz, *Annals of Physics* **152**, 239 (1984).
 - [5] G. Stefanucci and R. van Leeuwen, *Nonequilibrium Many-Body Theory of Quantum Systems: A Modern Introduction* (Cambridge University Press, Cambridge, 2013).
 - [6] K. Balzer and M. Bonitz, *Nonequilibrium Green's Functions Approach to Inhomogeneous Systems* (Springer, 2012).
 - [7] O. Konstantinov and V. Perel, *SOVIET PHYSICS JETP-USSR* **12**, 142 (1961).
 - [8] L. P. Kadanoff and G. A. Baym, *Quantum statistical mechanics: Green's function methods in equilibrium and nonequilibrium problems* (Benjamin, 1962).
 - [9] L. V. Keldysh et al., *Sov. Phys. JETP* **20**, 1018 (1965).
 - [10] N.-H. Kwong and M. Bonitz, *Phys. Rev. Lett.* **84**, 1768 (2000), URL <https://link.aps.org/doi/10.1103/PhysRevLett.84.1768>.
 - [11] N. E. Dahlen and R. van Leeuwen, *Phys. Rev. Lett.* **98**, 153004 (2007), URL <https://link.aps.org/doi/10.1103/PhysRevLett.98.153004>.
 - [12] K. Balzer, M. Bonitz, R. van Leeuwen, A. Stan, and N. E. Dahlen, *Phys. Rev. B* **79**, 245306 (2009), URL <https://link.aps.org/doi/10.1103/PhysRevB.79.245306>.
 - [13] P. Myöhänen, A. Stan, G. Stefanucci, and R. van Leeuwen, *EPL (Europhysics Letters)* **84**, 67001 (2008), URL <http://stacks.iop.org/0295-5075/84/i=6/a=67001>.
 - [14] P. Myöhänen, A. Stan, G. Stefanucci, and R. van Leeuwen, *Phys. Rev. B* **80**, 115107 (2009), URL <https://link.aps.org/doi/10.1103/PhysRevB.80.115107>.
 - [15] M. P. von Friesen, C. Verdozzi, and C.-O. Almbladh, *Phys. Rev. Lett.* **103**, 176404 (2009), URL <https://link.aps.org/doi/10.1103/PhysRevLett.103.176404>.
 - [16] M. Puig von Friesen, C. Verdozzi, and C.-O. Almbladh, *Phys. Rev. B* **82**, 155108 (2010), URL <https://link.aps.org/doi/10.1103/PhysRevB.82.155108>.
 - [17] K. Balzer, S. Bauch, and M. Bonitz, *Phys. Rev. A* **81**, 022510 (2010), URL <https://link.aps.org/doi/10.1103/PhysRevA.81.022510>.
 - [18] K. Balzer, S. Bauch, and M. Bonitz, *Phys. Rev. A* **82**, 033427 (2010), URL <https://link.aps.org/doi/10.1103/PhysRevA.82.033427>.
 - [19] M. Schüler, J. Berakdar, and Y. Pavlyukh, *Phys. Rev. B* **93**, 054303 (2016), URL <https://link.aps.org/doi/10.1103/PhysRevB.93.054303>.
 - [20] P. Lipavský, V. Špička, and B. Velický, *Phys. Rev. B* **34**, 6933 (1986), URL <https://link.aps.org/doi/10.1103/PhysRevB.34.6933>.
 - [21] S. Latini, E. Perfetto, A.-M. Uimonen, R. van Leeuwen, and G. Stefanucci, *Phys. Rev. B* **89**, 075306 (2014), URL <https://link.aps.org/doi/10.1103/PhysRevB.89.075306>.
 - [22] K. Pernal, O. Gritsenko, and E. J. Baerends, *Phys. Rev. A* **75**, 012506 (2007), URL <https://link.aps.org/doi/10.1103/PhysRevA.75.012506>.
 - [23] K. J. H. Giesbertz, O. V. Gritsenko, and E. J. Baerends, *The Journal of Chemical Physics* **133**, 174119 (2010), URL <https://doi.org/10.1063/1.3499601>.
 - [24] K. J. H. Giesbertz, O. V. Gritsenko, and E. J. Baerends, *The Journal of Chemical Physics* **140**, 18A517 (2014), URL <https://doi.org/10.1063/1.4867000>.
 - [25] M. Brics, J. Rapp, and D. Bauer, *Phys. Rev. A* **93**, 013404 (2016), URL <https://link.aps.org/doi/10.1103/PhysRevA.93.013404>.
 - [26] M. Brics, J. Rapp, and D. Bauer, *Journal of Physics B: Atomic, Molecular and Optical Physics* **50**, 144003 (2017), URL <http://stacks.iop.org/0953-4075/50/i=14/a=144003>.
 - [27] F. Lackner, I. Březinová, T. Sato, K. L. Ishikawa, and J. Burgdörfer, *Phys. Rev. A* **91**, 023412 (2015), URL <https://link.aps.org/doi/10.1103/PhysRevA.91.023412>.
 - [28] F. Lackner, I. Březinová, T. Sato, K. L. Ishikawa, and J. Burgdrfer, *Journal of Physics: Conference Series* **635**, 112084 (2015), URL <http://stacks.iop.org/1742-6596/635/i=11/a=112084>.
 - [29] S. Hermanns, N. Schlünzen, and M. Bonitz, *Phys. Rev. B* **90**, 125111 (2014), URL <https://link.aps.org/doi/10.1103/PhysRevB.90.125111>.
 - [30] N. Schlünzen and M. Bonitz, *Contrib. Plasma Phys.* **56**, 5 (2016), URL <http://dx.doi.org/10.1002/ctpp.201610003>.
 - [31] Y. Bar Lev and D. R. Reichman, *Phys. Rev. B* **89**, 220201 (2014), URL <https://link.aps.org/doi/10.1103/PhysRevB.89.220201>.
 - [32] G. Pal, Y. Pavlyukh, W. Hübner, and H. C. Schneider, *The European Physical Journal B* **79**, 327 (2011), URL <https://doi.org/10.1140/epjb/e2010-10033-1>.
 - [33] E. Perfetto, D. Sangalli, A. Marini, and G. Stefanucci, *Phys. Rev. B* **92**, 205304 (2015), URL <https://link.aps.org/doi/10.1103/PhysRevB.92.205304>.
 - [34] D. Sangalli, S. Dal Conte, C. Manzoni, G. Cerullo, and

- A. Marini, Phys. Rev. B **93**, 195205 (2016), URL <https://link.aps.org/doi/10.1103/PhysRevB.93.195205>.
- [35] E. A. A. Pogna, M. Marsili, D. De Fazio, S. Dal Conte, C. Manzoni, D. Sangalli, D. Yoon, A. Lombardo, A. C. Ferrari, A. Marini, et al., ACS Nano **10**, 1182 (2016), URL <https://doi.org/10.1021/acsnano.5b06488>.
- [36] Sangalli, D. and Marini, A., EPL **110**, 47004 (2015), URL <https://doi.org/10.1209/0295-5075/110/47004>.
- [37] E. Perfetto, D. Sangalli, A. Marini, and G. Stefanucci, Phys. Rev. B **94**, 245303 (2016), URL <https://link.aps.org/doi/10.1103/PhysRevB.94.245303>.
- [38] E. Perfetto, A.-M. Uimonen, R. van Leeuwen, and G. Stefanucci, Phys. Rev. A **92**, 033419 (2015), URL <https://link.aps.org/doi/10.1103/PhysRevA.92.033419>.
- [39] E. V. Boström, A. Mikkelsen, C. Verdozzi, E. Perfetto, and G. Stefanucci, Nano Lett. **18**, 785 (2018), URL <https://doi.org/10.1021/acs.nanolett.7b03995>.
- [40] E. Perfetto, D. Sangalli, A. Marini, and G. Stefanucci, The Journal of Physical Chemistry Letters **9**, 1353 (2018), URL <https://doi.org/10.1021/acs.jpclett.8b00025>.
- [41] F. Covito, E. Perfetto, A. Rubio, and G. Stefanucci, Phys. Rev. A **97**, 061401 (2018), URL <https://link.aps.org/doi/10.1103/PhysRevA.97.061401>.
- [42] J. M. Luttinger, Phys. Rev. **135**, A1505 (1964), URL <https://link.aps.org/doi/10.1103/PhysRev.135.A1505>.
- [43] F. G. Eich, A. Principi, M. Di Ventura, and G. Vignale, Phys. Rev. B **90**, 115116 (2014), URL <https://link.aps.org/doi/10.1103/PhysRevB.90.115116>.
- [44] F. G. Eich, M. Di Ventura, and G. Vignale, Phys. Rev. B **93**, 134309 (2016), URL <https://link.aps.org/doi/10.1103/PhysRevB.93.134309>.
- [45] F. Covito, F. G. Eich, R. Tuovinen, M. A. Sentef, and A. Rubio, Journal of Chemical Theory and Computation **14**, 2495 (2018), URL <https://doi.org/10.1021/acs.jctc.8b00077>.
- [46] M. Galperin, Chem. Soc. Rev. **46**, 4000 (2017), URL <http://dx.doi.org/10.1039/C7CS00067G>.
- [47] Y. Meir and N. S. Wingreen, Phys. Rev. Lett. **68**, 2512 (1992), URL <https://link.aps.org/doi/10.1103/PhysRevLett.68.2512>.
- [48] A.-P. Jauho, N. S. Wingreen, and Y. Meir, Phys. Rev. B **50**, 5528 (1994), URL <https://link.aps.org/doi/10.1103/PhysRevB.50.5528>.
- [49] M. Schüller and Y. Pavlyukh, Phys. Rev. B **97**, 115164 (2018), URL <https://link.aps.org/doi/10.1103/PhysRevB.97.115164>.
- [50] N. E. Dahlen and R. van Leeuwen, The Journal of Chemical Physics **122**, 164102 (2005), URL <https://doi.org/10.1063/1.1884965>.
- [51] K. Balzer, S. Hermanns, and M. Bonitz, EPL (Europhysics Letters) **98**, 67002 (2012), URL <http://stacks.iop.org/0295-5075/98/i=6/a=67002>.
- [52] N. Säkkinen, M. Manninen, and R. van Leeuwen, New Journal of Physics **14**, 013032 (2012), URL <http://stacks.iop.org/1367-2630/14/i=1/a=013032>.
- [53] M. Hopjan, D. Karlsson, S. Ydman, C. Verdozzi, and C.-O. Almbladh, Phys. Rev. Lett. **116**, 236402 (2016), URL <https://link.aps.org/doi/10.1103/PhysRevLett.116.236402>.
- [54] Y. B. Lev and D. R. Reichman, EPL (Europhysics Letters) **113**, 46001 (2016), URL <http://stacks.iop.org/0295-5075/113/i=4/a=46001>.
- [55] N. Schliinzen, J.-P. Joost, F. Heidrich-Meisner, and M. Bonitz, Phys. Rev. B **95**, 165139 (2017), URL <https://link.aps.org/doi/10.1103/PhysRevB.95.165139>.
- [56] A.-M. Uimonen, E. Khosravi, A. Stan, G. Stefanucci, S. Kurth, R. van Leeuwen, and E.K.U. Gross, Phys. Rev. B **84**, 115103 (2011).
- [57] C.-O. Almbladh, A. L. Morales, and G. Grossmann, Phys. Rev. B **39**, 3489 (1989), URL <https://link.aps.org/doi/10.1103/PhysRevB.39.3489>.
- [58] C.-O. Almbladh and A. L. Morales, Phys. Rev. B **39**, 3503 (1989), URL <https://link.aps.org/doi/10.1103/PhysRevB.39.3503>.
- [59] M. Cini, Solid State Communications **24**, 681 (1977), URL <http://www.sciencedirect.com/science/article/pii/0038109877903908>.
- [60] G. A. Sawatzky, Phys. Rev. Lett. **39**, 504 (1977), URL <https://link.aps.org/doi/10.1103/PhysRevLett.39.504>.
- [61] G. Stefanucci, S. Kurth, A. Rubio, and E. K. U. Gross, Phys. Rev. B **77**, 075339 (2008), URL <https://link.aps.org/doi/10.1103/PhysRevB.77.075339>.
- [62] G. Stefanucci, E. Perfetto, and M. Cini, Phys. Rev. B **81**, 115446 (2010), URL <https://link.aps.org/doi/10.1103/PhysRevB.81.115446>.
- [63] A. Kalvová, B. Velický, and V. Špička, EPL (Europhysics Letters) **121**, 67002 (2018), URL <http://stacks.iop.org/0295-5075/121/i=6/a=67002>.
- [64] E. Goulielmakis, Z.-H. Loh, A. Wirth, R. Santra, N. Rohringer, V. S. Yakovlev, S. Zherebtsov, T. Pfeifer, A. M. Azzeer, M. F. Kling, et al., Nature **466**, 739 (2010).
- [65] C. Bunge, J. Barrientos, and A. Bunge, Atomic Data and Nuclear Data Tables **53**, 113 (1993), ISSN 0092-640X, URL <http://www.sciencedirect.com/science/article/pii/S0092640X8371003X>.
- [66] J. Fernández Rico, I. Ema, R. López, G. Ramírez and K. Ishida, in *Recent Advances in Computational Chemistry: Molecular Integrals over Slater Orbitals*, eds. T. Ozdogan and M. B. Ruiz (Transworld Research Network, 2008), pp. 145.
- [67] J. F. Rico, R. López, I. Ema, and G. Ramirez, Journal of Computational Chemistry **25**, 1987 (2004), URL <https://onlinelibrary.wiley.com/doi/abs/10.1002/jcc.20131>.
- [68] P. Giannozzi, S. Baroni, N. Bonini, M. Calandra, R. Car, C. Cavazzoni, D. Ceresoli, G. L. Chiarotti, M. Cococcioni, I. Dabo, et al., Journal of Physics: Condensed Matter **21**, 395502 (2009), URL <http://stacks.iop.org/0953-8984/21/i=39/a=395502>.
- [69] N. Troullier and J. L. Martins, Phys. Rev. B **43**, 1993 (1991), URL <https://link.aps.org/doi/10.1103/PhysRevB.43.1993>.
- [70] J. P. Perdew, K. Burke, and M. Ernzerhof, Phys. Rev. Lett. **77**, 3865 (1996), URL <https://link.aps.org/doi/10.1103/PhysRevLett.77.3865>.
- [71] A. Marini, C. Hogan, M. Grüning, and D. Varsano, Computer Physics Communications **180**, 1392 (2009), URL <http://www.sciencedirect.com/science/article/pii/S0010465509000472>.
- [72] E. Clementi and C. Roetti, Atomic Data and Nuclear Data Tables **14**, 177 (1974), URL <http://www.sciencedirect.com/science/article/pii/S0092640X74800161>.
- [73] X. Andrade, D. Strubbe, U. De Giovannini, A. H. Larsen,

- M. J. T. Oliveira, J. Alberdi-Rodriguez, A. Varas, I. Theophilou, N. Helbig, M. J. Verstraete, et al., Phys. Chem. Chem. Phys. **17**, 31371 (2015), URL <http://dx.doi.org/10.1039/C5CP00351B>.
- [74] J. P. Perdew and A. Zunger, Phys. Rev. B **23**, 5048 (1981), URL <https://link.aps.org/doi/10.1103/PhysRevB.23.5048>.
- [75] E. Perfetto, A.-M. Uimonen, R. van Leeuwen, and G. Stefanucci, Journal of Physics: Conference Series **696**, 012004 (2016), URL <http://stacks.iop.org/1742-6596/696/i=1/a=012004>.
- [76] M. Ruberti, V. Averbukh, and P. Decleva, The Journal of Chemical Physics **141**, 164126 (2014), URL <https://doi.org/10.1063/1.4900444>.
- [77] M. Ruberti, P. Decleva, and V. Averbukh, Phys. Chem. Chem. Phys. **20**, 8311 (2018), URL <http://dx.doi.org/10.1039/C7CP07849H>.
- [78] M. Ruberti, P. Decleva, and V. Averbukh, Journal of Chemical Theory and Computation **0**, null (0), URL <https://doi.org/10.1021/acs.jctc.8b00479>.
- [79] H. Y. Fan, Phys. Rev. **82**, 900 (1951), URL <https://link.aps.org/doi/10.1103/PhysRev.82.900>.